

SPECTROSCOPIC REDSHIFTS OF GALAXIES WITHIN THE FRONTIER FIELDS

HARALD EBELING¹, CHENG-JIUN MA^{1,2,3,4}, ELIZABETH BARRETT¹

(Received September 24, 2013; Accepted February 7, 2014)

ABSTRACT

We present a catalog of 1921 spectroscopic redshifts measured in the fields of the massive galaxy clusters MACSJ0416.1–2403 ($z = 0.397$), MACSJ0717.5+3745 ($z = 0.546$), and MACSJ1149.5+2223 ($z = 0.544$), i.e., three of the four clusters selected by STScI as the targets of the Frontier Fields (FF) initiative for studies of the distant Universe via gravitational lensing. Compiled in the course of the MACS project (Massive Cluster Survey) that detected the FF clusters, this catalog is provided to the community for three purposes: (1) to allow the identification of cluster members for studies of the galaxy population of these extreme systems, (2) to facilitate the removal of unlensed galaxies and thus reduce shear dilution in weak-lensing analyses, and (3) to improve the calibration of photometric redshifts based on both ground- and spacebased observations of the FF clusters.

Subject headings: galaxies: clusters: individual (MACSJ0416.1–2403, MACSJ0717.5+3745, MACSJ1149.5+2223); galaxies: distances and redshifts

1. INTRODUCTION

Recognizing the importance of massive galaxy clusters as gravitational telescopes for studies of the distant universe as originally proposed by the Clusters as Telescopes team (CATs⁵), Space Telescope Science Institute (STScI) recently announced the Frontier Fields (FF) project, a commitment of 560 orbits of *Hubble Space Telescope* (*HST*) time in Cycles 21 and 22 to deep observations of four clusters of galaxies at intermediate redshift ($0.3 < z < 0.6$). Each target will be observed with both the Advanced Camera for Surveys (ACS) and the Wide Field Camera 3 (WFC3) for 20 orbits in each of the F435W, F606W, F814W, F105W, F125, F140, and F160W filters, reaching a limiting magnitude of approximately 29 (AB system) across the full optical and near-infrared (NIR) window. Both ACS and WFC3 will be used simultaneously, such that for each cluster target images of equal depth are accumulated of the cluster core and of a flanking parallel field about 6 arcmin away. Extending the NIR spectral coverage further, 1000 hours of Spitzer Space Telescope time are being devoted to observations of the same four fields at 3.6 and 4.5 μm .

The FF project represents the largest investment of *HST* time for deep observations of galaxy clusters in the history of *HST*. Its main science goal is the discovery of gravitationally lensed background galaxies at $z = 5 - 10$ for both in-depth studies of bright individual objects and statistical investigations into the properties of galaxies at magnitudes and distances inaccessible to observation without gravitational amplification. As a bonus, the FF observations will also yield the deepest images of the cores of massive clusters ever collected, thereby facilitating exquisitely detailed characteriza-

tions of the cluster lenses and their galaxy content.

The four clusters selected for the FF initiative for Cycle 21 and 22 are A2744 ($z=0.308$), MACSJ0416.1–2403 ($z=0.397$), MACSJ0717.5+3745 ($z=0.546$), and MACSJ1149.5+2223 ($z=0.544$) (Abell 1958; Edge et al. 2003; Ebeling et al. 2007, 2010; Mann & Ebeling 2012). Subject to a review of the observations collected up to then, two additional clusters (AS1063 and A370) will be added to the FF sample and observed in Cycle 23. All FF clusters are exceptionally X-ray luminous systems ($L_X > 2 \times 10^{45}$ erg s⁻¹, bolometric) and feature pronounced substructure, i.e., they combine the two characteristics that select the most powerful cluster lenses (Horesh et al. 2010; Limousin et al. 2012; Zitrin et al. 2013). Additional information on the FF project can be found on <http://www.stsci.edu/hst/campaigns/frontier-fields/>.

2. CHARACTERIZING THE FF LENSES

If the scientific potential of the FF project for the characterization of the high-redshift Universe is to be fully exploited, the magnification of the cluster lenses and thus their mass distributions must be accurately mapped. Within the cluster cores, the mass distribution can be derived from carefully identified strong-gravitational lensing features, with the greatest leverage being provided by sets of multiple-image systems (Kneib & Natarajan 2011, and references therein). In addition to cluster-scale halos, the resulting mass models also include appropriately scaled mass halos at the location of the most luminous cluster galaxies, thereby accounting for small-scale perturbations. On larger scales, i.e., outside the strong-lensing regime, complementary constraints on the mass and magnification maps are obtained from measurements of the weak gravitational shear induced by the cluster lens. For the FF clusters, the weak-lensing regime is poorly sampled by the pre-FF, relatively shallow *HST* images; better coverage and thus better constraints on the mass and magnification at larger cluster-centric radii will ultimately emerge from the much deeper FF images themselves (including those of the flanking fields) as well as from supporting wide-field imaging.

In preparation of the forthcoming FF observations with *HST*, STScI assigned in the summer of 2013 six teams the task of generating maps of the mass distribution of, and grav-

¹ Institute for Astronomy, University of Hawaii, 2680 Woodlawn Drive, Honolulu, HI 96822, USA

² Department of Physics & Astronomy, University of Waterloo, 200 University Ave. W., Waterloo, Ontario, N2L 3G1, Canada

³ Harvard-Smithsonian Center for Astrophysics, 60 Garden St., Cambridge, MA, 021380-1516, USA

⁴ Institute for Computational Cosmology, Durham University, South Road, Durham, DH1 3LE, UK

⁵ Led by Jean-Paul Kneib, the CATs team consists of cluster and lensing experts from the US and Europe; CATs was one of six teams selected by STScI in the spring of 2013 to calibrate the FF cluster lenses.

Run ID	Date	Telescope/Instrument	Grating or Grism	Central Wavelength (Å)	Blocking Filter	Exposure Time (s)	Spectral Resolution (Å)
L1	2000-11-20/21	Keck-I/LRIS	400/3400, 600/7500	6200	GG495	3600 (e1) 4800 (e2)	6.8, 4.7
L2	2002-11-29	Keck-I/LRIS	400/3400, 600/7500	6500	GG495	5400 (e1) 6000 (e2)	6.8, 4.7
D1	2003-12-23	Keck-II/DEIMOS	600ZD	6500	GG495	7200	6.5
G1	2004-03-12	Gemini/GMOS	B600	6700	GG455	5400	4.7
G2	2004-03-17	Gemini/GMOS	R400	7600	OG515	7200	6.9
D2	2004-12-16	Keck-II/DEIMOS	600ZD	7000	GG455	5400	5.7
D3	2005-02-12	Keck-II/DEIMOS	600ZD	7000	GG455	3240 (e1) 7310 (e2)	5.7
D4	2006-01-31	Keck-II/DEIMOS	600ZD	7000	GG455	6047 (e1) 5400 (e2) 4992 (e3) 5100 (e4)	5.7
D5	2006-02-01	Keck-II/DEIMOS	600ZD	7000	GG455	3600 (e1) 5400 (e2)	5.7
D6	2006-12-22	Keck-II/DEIMOS	600ZD	7000	GG455	5400	4.5
D7	2008-01-05/06/07	Keck-II/DEIMOS	600ZD	6300	GG455	5400 (e1) 7200 (e2)	4.5

TABLE 1
OBSERVING RUNS AND INSTRUMENTAL SETUP FOR OUR SPECTROSCOPIC FOLLOW-UP OBSERVATIONS OF GALAXIES IN THE FIELD OF MACSJ0717.5+3745. THE EFFECTIVE SPECTRAL RESOLUTION AS LISTED REPRESENTS THE FWHM OF AN ARC LINE.

Run ID	Date	Telescope/Instrument	Grating or Grism	Central Wavelength (Å)	Blocking Filter	Exposure Time (s)	Spectral Resolution (Å)
G1	2003-05-01	Gemini/GMOS	B600	5900	OG515	3600	4.7
G2	2004-03-16	Gemini/GMOS	R400	7600	OG515	7200	6.9
D1	2005-02-12	Keck-II/DEIMOS	600ZD	7000	GG455	5400	5.7
D2	2006-04-30	Keck-II/DEIMOS	600ZD	7000	GG455	2700 (e1) 4800 (e2) 5400 (e3)	5.7
D3	2009-02-26	Keck-II/DEIMOS	600ZD	6700	GG455	2150 (e1) 3600 (e2)	5.7

TABLE 2
LIKE TABLE 1 BUT FOR OUR OBSERVATIONS OF MACSJ1149.5+2223.

itional amplification provided by, the FF clusters, based on strong- and weak-lensing analyses of the pre-FF *HST* imaging data (e.g. Richard et al., in preparation). Spectroscopic follow-up observations from the ground were critical in this effort, not only to robustly anchor the lens models via spectroscopic redshifts of multiple-image systems, but also to unambiguously identify cluster members among the galaxies in the FF fields. The latter play an important role as small-scale perturbers of the strong-lensing mass models, and are essential also for the elimination of unlensed galaxies in the weak-lensing analysis.

In the following we briefly describe spectroscopic follow-up work conducted by us in the fields of three of the four approved FF clusters as part of our extensive spectroscopic survey of the galaxy population of cluster discovered by the Massive Cluster Survey (MACS; Ebeling et al. 2001). Since the underlying MACS follow-up observations served various scientific purposes, the instrumental settings differed between observing runs, the spectra obtained vary in resolution and wavelength coverage, and the combined survey results are not statistically complete. The inhomogeneity of this data set notwithstanding, we hope that the information provided here will prove useful for the extragalactic community. All redshifts have previously been made available to the six teams generating mass and magnification maps of the FF from pre-FF data.

3. SPECTROSCOPIC OBSERVATIONS

A2744 (MACSJ0014.3–3022; Ebeling et al. 2010) was not targeted in the spectroscopic follow-up observations conducted by the MACS team, as the system (also known as AC118) has been covered extensively before (Couch & Sharples 1987; Couch et al. 1998; Boschin et al. 2006; Owers et al. 2011). Galaxies with spectroscopic redshifts listed in the compilation of Owers et al. (2011) are marked in Fig. 1 (top).

MACSJ0416.1–2403 was observed by us on January 20, 2001 with the multi-object spectrograph (MOS) on the Canada-Hawaii-France Telescope (CFHT) on Mauna Kea, Hawaii. Our instrumental setup combined the B300 grism with the EEV1 CCD, resulting in a pixel scale of 3.3Å pixel^{-1} and an effective resolution of 12.5Å (as determined by the FWHM of an arc line). We observed a single MOS mask for a total integration time of 6000 s. Since the goal of these observations was to obtain a credible global velocity dispersion of the cluster, which requires spectra for as many cluster members as possible, the 4504V broadband filter was inserted into the light path, thereby limiting the wavelength range of the resulting spectra to 876Å centred on 5468Å . The truncated spectra could then be stacked in three to four tiers along the dispersion direction, allowing us to observe many more galaxies on a single MOS mask than would otherwise have been possible. The narrow spectral range covered ensured that red-

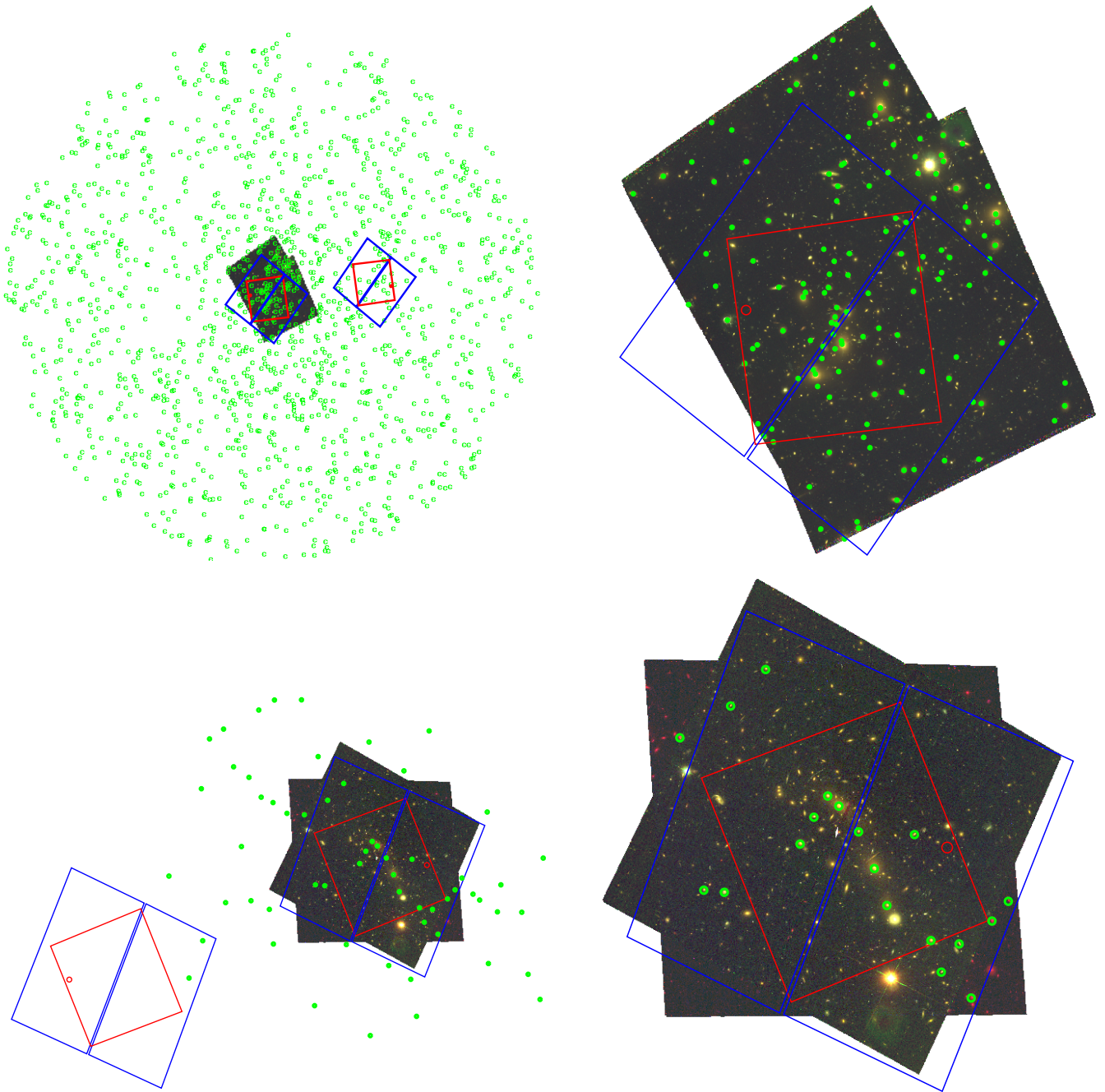


FIG. 1.— Color images (F435W+F606W+F814W) of the archival *HST* data for the FF. Top: A2744, bottom: MACSJ0416.1–2403. Galaxies with spectroscopic redshifts are marked by green circles. For either cluster, the left panel shows the full extent of the spectroscopic data set discussed in Section 3, while the right panel shows a closeup of the data within the area covered by the pre-FF *HST* images of the FF. Overlaid in blue (red) are the apertures of the planned, deep FF observations with ACS (WFC3).

shifts could be obtained from the Ca H+K lines for galaxies at the approximate cluster redshift of $z = 0.4$, but did not allow the detection and measurement of most other spectral diagnostics (G band, $H\beta$, [OIII], etc.)

MACSJ0717.5+3745 and *MACSJ1149.5+2223* are part of the subsample of MACS clusters at $z > 0.5$ (Ebeling et al. 2007), and were observed extensively by us, primarily in the context of a study of the impact of environment on spectral and morphological properties of the cluster galaxy population (Ma et al. 2008; Ma & Ebeling 2011). We list the respective observing runs and details of the instrumental setup in

Tables 1 and 2 for our observations of *MACSJ0717.5+3745* and *MACSJ1149.5+2223*, respectively. All observations were performed using multi-object spectrographs on telescopes on Mauna Kea, Hawaii. The vast majority of our spectroscopic data were collected with DEIMOS on Keck-II, using the 600ZD grating. With this setup, the spectral range covered is independent of the chosen central wavelength (which varied between 6300 and 7000Å); instead, it is determined by the choice of order-blocking filter and by the location of a given slit on the respective MOS mask. For a centrally located slit, the usable wavelength range is approximately 4700

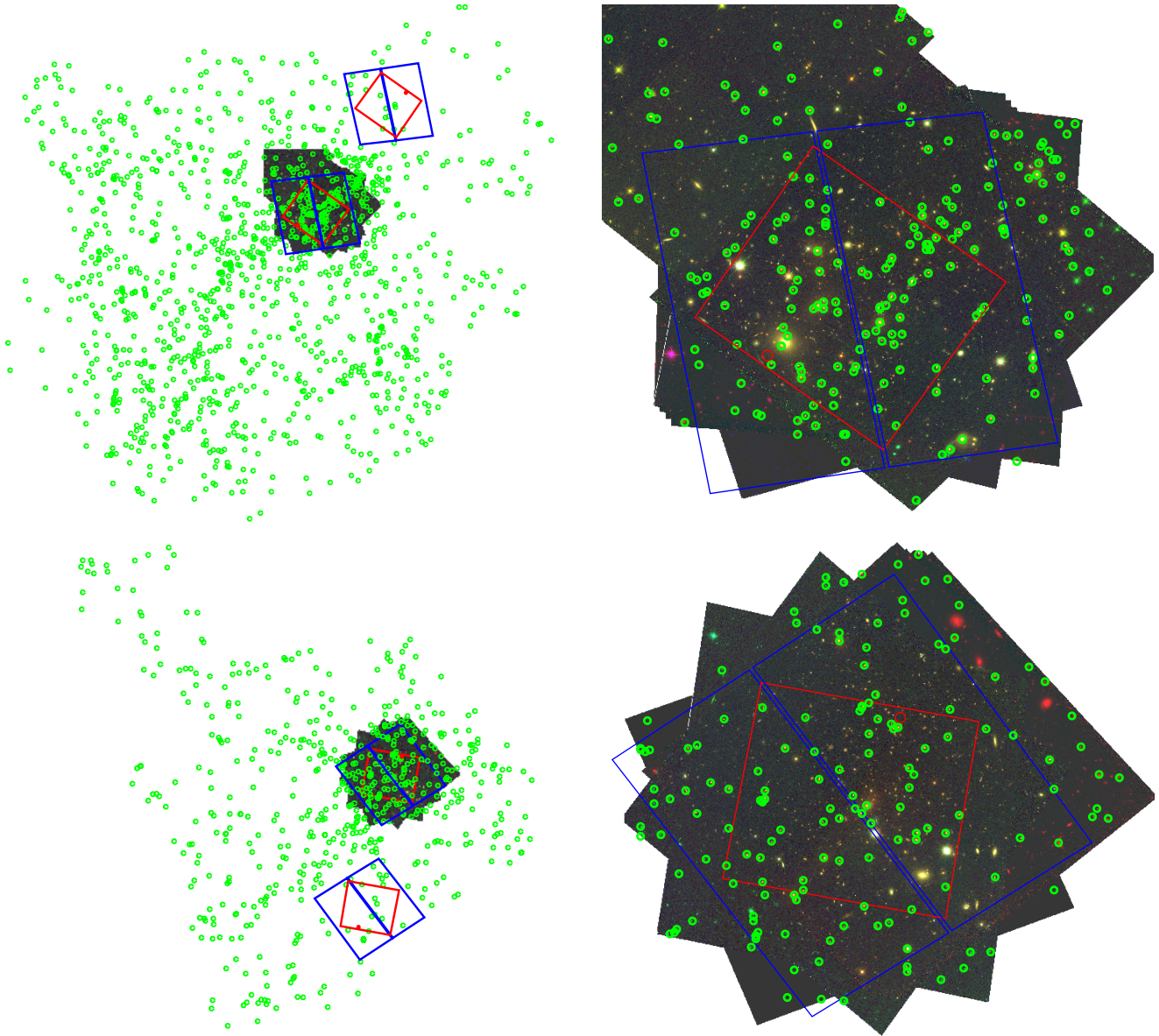


FIG. 2.— As Fig. 1 but for MACSJ0717.5+3745 (top) and MACSJ1149.5+2223 (bottom). The north-eastern quadrant of the image for MACSJ0717.5+3745 includes a small section of the much larger 3×6 *HST/ACS* mosaic in the F555W and F814W filters obtained by program GO-10420 (PI Ebeling) and designed to cover the large-scale filament extending to the south-east of the cluster core (Jauzac et al. 2012).

(5200) to 8800Å (9800Å) for the GG455 (GG495) blocking filter. The effective spectral resolution of our DEIMOS data is typically 6Å. Spectra were also obtained using LRIS on Keck-I, using the 400/3400 grism in the blue arm, and the 600/7500 grating in the red arm of the spectrograph. Finally, MACSJ0717.5+3745 and MACSJ1149.5+2223 were observed by us with GMOS on Gemini-N, using the EEV detector array as well as the B600 and R400 gratings, which feature comparable efficiency at 6000 to 7000Å. Use of the GG495 (OG515) order-blocking filter with the B600 (R400) grating results in a usable spectral range of approximately 5300–8100Å (5400–9600Å); the spectral coverage is slightly extended or truncated at the blue or red end of this range for slits placed near the edges of the MOS masks. Additional instrumental details, largely similar to the ones used with DEIMOS, can be found in Tables 1 and 2.

4. DATA REDUCTION

Generic data reduction procedures were applied to data collected from all telescopes, including bias subtraction, cosmic-ray removal via median averaging of at least three frames where possible, flat fielding, wavelength calibration, skyline straightening, aperture extraction, and background subtraction. Following bias subtraction, trimming, and median combining, data for each slit were extracted from the spectral image and analyzed individually thereafter. Dispersion solutions were obtained using standard calibration lamps (Cu, Cd, Zn, Hg, Kr, Ne, Ar). Skyline straightening was performed when required, and dispersion solutions were verified via comparison to telluric emission lines. Finally, object spectra were extracted for each aperture and a locally determined background was subtracted.

For data obtained with CFHT/MOS these reduction steps were performed using the respective *IRAF* tools; for data ob-

tained with Keck and Gemini, use was made of the telescope-specific Keck-II/DEIMOS pipeline developed by the DEEP2 team (Cooper et al. 2012; Newman et al. 2013) and its adaptation Low-Redux (for Keck-I/LRIS and Gemini/GMOS).

Since multi-slit masks were used for all observations, flux calibration using standard stars cannot trivially be applied, and redshifts were measured from absorption and emission features using cross correlations of the observed spectra with spectral templates (e.g., Le Fèvre et al. 2005). In all cases, the resulting redshifts were verified manually using at least two prominent spectral features, such as (in absorption) Ca H and K, H δ , or the G band, and (in emission) [O II] λ 3727, H β , and [O III] λ 4959, 5007.

The accuracy of our redshift measurements is limited by the signal-to-noise ratio (S/N) of our spectra as well as by the precision of their wavelength calibration. The latter introduces a systematic uncertainty dz of about 0.0002. We estimate the impact of S/N by comparing the redshifts measured for over 150 galaxies that were observed more than once and feature spectra of comparable S/N. Accounting for the noise in the observed correlation between S/N and redshift differential between repeat measurements, we group all spectra into three

broad S/N classes. The standard deviations of the distribution of redshift differentials for these three groups are measured to be $dz=0.0003$, 0.0005 , and 0.001 , and are consequently assigned as the empirical, 1σ redshift uncertainties to spectra with high, medium, and low S/N.

5. RESULTS

Table 3 lists the coordinates, redshifts, redshift uncertainties, and spectral types (absorption-line, emission-line, and E+A spectra) of the 65 galaxies successfully observed by us with CFHT in the field of MACSJ0416.1–2403. The results from our spectroscopic survey of galaxies in the fields of MACSJ0717.5+3745 (1266 redshifts) and MACSJ1149.5+2223 (590 redshifts) are shown in the same format in Tables 4 and 5 for the first 20 galaxies (in R.A. order) in each field. The full set of results can be obtained electronically from the ApJ website.

ACKNOWLEDGEMENTS

HE gratefully acknowledges financial support from STScI grants GO-9722 and GO-10420. The *HST* images of the FF shown in Figs. 1 and 2 were reduced and kindly made available by Anton Koekemoer.

REFERENCES

- G. O. Abell, 1958, *ApJS*, 3, 211
 Boschin W., Girardi M., Spolaor M., Barrena R., 2006, *A&A*, 449, 461
 Cooper M., Newman J.A., Davis M., Finkbeiner D.P., Gerke B.F., 2012, ASCL, 1203.003
 Couch W.J. & Sharples R.M., 1987, *MNRAS*, 229, 423
 Couch W.J., Barger A.J., Smail I., Ellis R.S., Sharples R.M., 1998, *ApJ*, 497, 188
 Ebeling H., Edge A.C., Henry J.P., 2001, *ApJ*, 553, 668
 Ebeling H., Barrett E., Donovan D., Ma C.-J., Edge A. C., Van Speybroeck L., 2007, *ApJ*, 661, L33
 Ebeling H., Edge A. C., Mantz A., Barrett E., Henry J. P., Ma C. J., van Speybroeck L., 2010, *MNRAS*, 407, 83
 Edge, A. C., Ebeling, H., Bremer, M., et al. 2003, *MNRAS*, 339, 913
 Horesh, A., Maoz, D., Ebeling, H., Seidel, G., & Bartelmann, M. 2010, *MNRAS*, 406, 1318
 Jauzac M., et al., 2012, *MNRAS*, 426, 3369
 Kneib J.-P. and Natarajan P., 2011, *AAPR*, 18, 47
 Le Fèvre, O., Vettolani, G., Garilli, B., et al. 2005, *A&A*, 439, 845
 Limousin, M., Ebeling, H., Richard, J., et al. 2012, *A&A*, 544, A71
 Ma C.-J., Ebeling H., 2011, *MNRAS*, 410, 2593
 Ma C.-J., Ebeling H., Donovan D., Barrett E., 2008, *ApJ*, 684, 160
 Mann A.W. & Ebeling H., 2012, *MNRAS*, 420, 2120
 Newman J.A. et al., 2013, *ApJS*, 208, 5N
 Owers M.S., Randall S.W., Nulsen P.E.J., Couch W.J., David L.P., Kempner J.C., 2011, *ApJ*, 728, 27
 Zitrin, A., Meneghetti, M., Umetsu, K., et al. 2013, *ApJ*, 762, L30

name	z	DQ	ST	name	z	DQ	ST	name	z	DQ	ST
MACSg J041549.35-240512.6	0.3050	3	A	MACSg J041604.82-240538.8	0.3844	2	A	MACSg J041614.82-240722.7	0.3947	2	A
MACSg J041549.59-240250.2	0.3965	1	A	MACSg J041605.26-240520.7	0.3944	1	A	MACSg J041615.74-240324.7	0.3121	1	A
MACSg J041550.24-240257.6	0.2817	2	A	MACSg J041605.53-240736.0	0.3902	1	A	MACSg J041616.00-240101.4	0.2754	2	A
MACSg J041550.35-240710.5	0.3761	2	A	MACSg J041605.95-240420.1	0.3976	1	A	MACSg J041617.33-240323.0	0.4058	3	A
MACSg J041552.15-240430.1	0.4031	3	A	MACSg J041606.06-240649.9	0.3961	1	A	MACSg J041618.47-240101.7	0.3896	3	A
MACSg J041553.00-240717.0	0.3560	1	A	MACSg J041606.67-240229.9	0.3974	3	A	MACSg J041618.57-240605.8	0.3574	1	A
MACSg J041553.98-240418.6	0.4002	3	A	MACSg J041607.09-240500.6	0.3970	1	A	MACSg J041618.61-240309.5	0.3897	1	A
MACSg J041554.27-240715.0	0.3553	1	A	MACSg J041607.62-240439.5	0.3963	1	A	MACSg J041618.93-240522.6	0.2806	1	A
MACSg J041555.36-240643.6	0.3937	1	A	MACSg J041608.05-240632.6	0.3988	1	A	MACSg J041619.68-240302.8	0.4000	1	A
MACSg J041555.94-240526.3	0.3965	1	A	MACSg J041608.28-240418.5	0.4008	2	A	MACSg J041619.90-240114.1	0.4004	3	A
MACSg J041557.83-240452.0	0.4002	3	A	MACSg J041609.10-240403.8	0.4002	1	A	MACSg J041620.61-240511.8	0.3991	2	A
MACSg J041558.16-240525.8	0.3761	3	A	MACSg J041609.57-240358.0	0.3950	1	A	MACSg J041620.79-240238.0	0.3918	2	A
MACSg J041558.98-240630.1	0.4089	3	A	MACSg J041609.75-240800.1	0.3430	1	A	MACSg J041621.48-240404.3	0.3984	1	A
MACSg J041559.10-240321.3	0.3904	1	A	MACSg J041609.85-240154.1	0.4004	3	A	MACSg J041622.19-240224.8	0.3890	1	A
MACSg J041559.78-240511.0	0.3070	1	A	MACSg J041610.15-240410.3	0.3996	1	A	MACSg J041622.92-240514.3	0.3972	1	A
MACSg J041600.38-240503.7	0.3072	1	A	MACSg J041610.72-240425.5	0.4031	3	A	MACSg J041623.10-240137.7	0.3898	3	E
MACSg J041601.39-240443.6	0.3945	1	A	MACSg J041611.92-240606.5	0.3926	1	A	MACSg J041624.38-240150.1	0.4012	3	A
MACSg J041602.02-240458.3	0.4016	2	A	MACSg J041612.16-240245.8	0.3865	1	A	MACSg J041625.01-240601.7	0.3960	1	A
MACSg J041602.70-240509.6	0.3962	1	A	MACSg J041613.62-240306.7	0.3923	1	A	MACSg J041625.13-240252.3	0.3981	1	A
MACSg J041603.57-240553.5	0.4000	1	A	MACSg J041613.89-240453.2	0.3533	1	E	MACSg J041626.26-240648.3	0.4123	2	A
MACSg J041604.07-240522.7	0.3960	1	A	MACSg J041614.50-240212.1	0.4020	3	A	MACSg J041628.08-240441.1	0.4003	1	A
MACSg J041604.39-240140.2	0.3967	1	A	MACSg J041614.74-240451.9	0.3118	1	A				

TABLE 3

SPECTROSCOPIC REDSHIFTS MEASURED AT CFHT FOR 65 GALAXIES IN THE FIELD OF MACSJ0416.1–2403. THE FINAL 18 CHARACTERS OF THE NAME REPRESENT THE OBJECT’S EQUATORIAL COORDINATES FOR THE J2000 EQUINOX. THE DATA QUALITY (DQ) INDICATOR IN THE THIRD COLUMN PROVIDES AN ESTIMATE OF THE MEASUREMENT ACCURACY; A VALUE OF 1, (2, 3) TRANSLATES INTO A 1σ UNCERTAINTY OF APPROXIMATELY 0.0003 (0.0005, 0.001) IN THE REDSHIFT OF THE RESPECTIVE GALAXY. THE SPECTRAL TYPE (ST) IS LISTED IN THE FINAL COLUMN; WE DISTINGUISH BETWEEN ABSORPTION-LINE SPECTRA (A), EMISSION-LINE SPECTRA (E), AND E+A GALAXIES (E+A).

name	z	DQ	ST	Instrument
MACSg J071639.04+374808.3	0.3498	1	E	D
MACSg J071642.04+374852.6	0.3349	1	E	D
MACSg J071644.13+374601.5	0.3349	1	A	D
MACSg J071644.50+374921.0	0.3351	1	E	D
MACSg J071644.58+374542.2	0.2603	1	A	D
MACSg J071644.81+374734.5	0.4610	1	A	D
MACSg J071644.93+374900.8	0.3358	1	E+A	D
MACSg J071645.64+374123.5	0.5426	1	A	D
MACSg J071645.96+374622.3	0.6130	1	E	D
MACSg J071647.05+374008.1	0.5382	1	E	D
MACSg J071647.34+374107.7	0.5436	1	E	D
MACSg J071647.59+374007.7	0.3665	1	E	D
MACSg J071647.91+374652.6	0.4611	1	E	D
MACSg J071648.22+374540.5	0.4023	1	E	D
MACSg J071649.25+375121.7	0.5137	2	E	D
MACSg J071649.35+374018.2	0.5433	1	A	D
MACSg J071649.45+374544.4	0.5150	1	E	D
MACSg J071650.86+374618.5	0.3352	2	E	D
MACSg J071651.01+374206.9	0.3343	1	E	D
MACSg J071651.40+375235.1	0.4200	2	E	D

TABLE 4

SPECTROSCOPIC REDSHIFTS FOR 1266 GALAXIES IN THE FIELD OF MACSJ0717.5+3745. COLUMNS AS IN TABLE 3, EXCEPT THAT WE ALSO LIST THE INSTRUMENT USED (D FOR KECK/DEIMOS, L FOR KECK/LRIS, G FOR GEMINI-N/GMOS). WE LIST ONLY THE FIRST 20 GALAXIES; THE FULL SET IS AVAILABLE ONLINE.

name	z	DQ	ST	Instrument
MACSg J114909.03+222346.2	0.5961	3	E	D
MACSg J114909.38+222107.5	0.9309	3	E	D
MACSg J114910.30+222207.7	0.5644	2	E	D
MACSg J114910.99+222031.6	0.5654	1	E	D
MACSg J114911.06+222030.7	0.5643	1	E	D
MACSg J114911.20+222128.1	0.9351	3	E	D
MACSg J114913.28+222004.3	0.5673	2	E	D
MACSg J114913.40+222414.9	0.5342	1	A	D
MACSg J114913.62+222045.3	0.4549	1	E	D
MACSg J114913.83+222520.3	0.5495	1	A	D
MACSg J114914.74+222413.9	0.5351	1	E	D
MACSg J114914.86+222200.8	0.6912	2	E	D
MACSg J114914.97+222123.7	0.4585	1	A	D
MACSg J114915.11+222215.9	0.5471	2	E+A	D
MACSg J114915.19+222355.8	0.5339	1	E	D
MACSg J114915.33+222341.0	0.5340	2	E	D
MACSg J114915.71+222120.7	0.4558	3	A	D
MACSg J114916.15+222147.3	0.6639	2	A	D
MACSg J114916.19+222114.5	0.5422	1	A	D
MACSg J114916.38+222425.7	0.5429	2	A	D

TABLE 5

SPECTROSCOPIC REDSHIFTS FOR 590 GALAXIES IN THE FIELD OF MACSJ1149.5+2223. COLUMNS AS IN TABLE 4. WE LIST ONLY THE FIRST 20 GALAXIES; THE FULL SET IS AVAILABLE ONLINE.